

# Baryon spectroscopy: Recent results from the Crystal Barrel/TAPS experiment at ELSA

U. Thoma

for the CBELSA/TAPS Collaboration

*Helmholtz-Institut für Strahlen- und Kernphysik, Universität Bonn, Germany*

**Abstract.** To understand the spectrum and the properties of baryon resonances, the CBELSA/TAPS experiment at ELSA investigates the photoproduction of single- and multi-meson final states off the nucleon. In the latter final states baryon cascades via  $\Delta\pi$  and  $\Delta\eta$  and also via higher mass baryon resonances are clearly observed. A partial wave analysis based on single and double meson photoproduction data as well as data from other reactions allows a first determination of resonance properties including partial decay widths of various  $N^*$  and  $\Delta^*$  states. Those include also the decays into the different  $p\pi^0\pi^0$  and  $p\pi^0\eta$  decay channels resulting partly in unexpected results. Recently not only single but also double polarisation experiments have been performed, which are absolutely necessary to resolve ambiguities in the partial wave analyses (PWA) used to extract the resonances from the data; without the measurement of polarisation observables a model-independent PWA will not be possible. Polarisation observables have been investigated using linearly, circularly polarized or unpolarized photons impinging on an longitudinally polarized or unpolarized target. Given the angular coverage of the Crystal-Barrel/TAPS experiment this data cover almost the full angular range and phase space. This data will provide key information for the partial wave analyses and brings us one step closer towards the needed complete experiment.

**Keywords:** Baryon resonances, Photoproduction, Polarization observables

**PACS:** 13.60.-r, 13.60.Le, 13.88.+e

## INTRODUCTION

To understand the non-perturbative regime of QCD – the world of the nucleon and its excitations – is still among the most exciting challenges in subnuclear physics. In the past most of the information on the baryon excitation spectrum was obtained from  $\pi N$ -scattering experiments putting a clear bias on resonances with a sizeable  $\pi N$ -coupling. Recently this data were supplemented by photo- and electroproduction data, which offers the opportunity to study resonances with vanishing  $\pi N$ -coupling in reactions such as e.g.  $\gamma p \rightarrow p\eta$ . To extract the broad and strongly overlapping resonances from the data two issues are rather important: First of all, polarisation observables need to be measured to gain enough constraints for an unambiguous extraction of the contributing amplitudes from the data. Secondly, different final states need to be investigated since different resonances may couple with rather different strength to different final states making their observation more probable in certain reactions compared to others. This of course includes measurements of single-meson photoproduction reactions as well as the more complicated multi-meson photoproduction. The latter gets more and more important at higher energies. In addition to the spectrum of resonances also their properties are of interest. The measurement of decay modes provides important information to distinguish between different models trying to describe the baryon spectrum such as e.g. the quark model or calculations investigating the option of dynamically generated resonances. The ground state baryons and the low-mass excitations evidence the decisive role of SU(3) symmetry and suggest an interpretation of the spectrum in constituent quark models [1, 2, 3]. Baryon decays can be calculated in quark models using harmonic-oscillator wave functions and assuming a  $q\bar{q}$  pair creation operator for meson production. A comprehensive review of predictions of baryon masses and decays can be found in [4]. An alternative description of the baryon spectrum may be developed in effective field theories in which baryon resonances are generated dynamically from their decays [5, 6]. At present, the approach is restricted to resonances coupling to octet baryons and pseudoscalar mesons, yet it can possibly be extended to include vector mesons and decuplet baryons [7]. To test the different approaches, detailed information on the spectrum and decays of resonances is needed, including also more complex decay modes such as e.g.  $\Delta\pi$ ,  $\Delta\eta$  or  $N(\pi\pi)$ - $S$ -wave, accessible via the investigation of the reactions  $\gamma p \rightarrow p\pi^0\pi^0$  and  $\gamma p \rightarrow p\pi^0\eta$ . A recent review on the subject of baryon spectroscopy can be found in [9].

## SINGLE-MESON PHOTOPRODUCTION: $\gamma p \rightarrow p\eta$

The Crystal Barrel detector is very well suited to measure neutral mesons decaying into photons. Therefore  $\eta$ -decays either into two photons or  $3\pi^0$  are investigated. The according invariant mass spectra (Fig. 1) show clear signals over an almost negligible ( $\eta \rightarrow 2\gamma$ ) or small background ( $\eta \rightarrow 3\pi^0$ ). Photoproduction of  $\eta$ -mesons is an interesting reaction to investigate the baryon spectrum. The  $\eta$  meson as isospin zero particle acts as isospin filter; only baryon resonances with isospin  $I=1/2$  can contribute. While all the partial wave analyses (PWA) used to extract the resonances agree on the

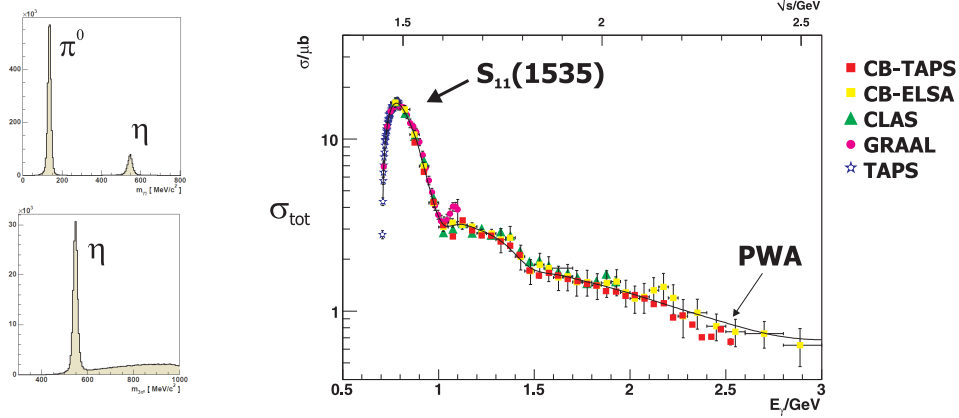


**FIGURE 1.** Left:  $2\gamma$  and  $3\pi^0$  invariant mass distributions. Right: Total  $\gamma p \rightarrow p\eta$  cross section for the CBELSA/TAPS-data [8] in comparison to previous CB-ELSA [10], GRAAL [11] and TAPS [12] data. Solid line: result the BnGa-partial wave analysis [13].

$S_{11}(1535)$ -dominance at threshold (Fig. 1) already in the third resonance region clear differences in the interpretation of the data occur. In the  $\eta$ -MAID model, the  $P_{11}(1710)$  [14] provides a rather significant contribution in this mass range. In the Bonn-Gatchina (BnGa) PWA [13], which includes CB-ELSA data from various reactions as well as data from other experiments, three dominating nucleon resonance contributions have been found: the  $S_{11}(1535)$ , the  $P_{13}(1720)$ , and in addition a newly proposed state, the  $D_{15}(2070)$  [13]. Even though in both models the differential cross sections as well as the beam asymmetry  $\Sigma$  data (Fig.3) are both well described, the contributing partial waves are still rather different. Further observables need to be measured; observables with polarized beam and polarized target will be a key.

## MULTI-MESON PHOTOPRODUCTION: $\gamma p \rightarrow p\pi^0\pi^0$

Multi-meson final states like  $\gamma p \rightarrow p\pi^0\pi^0$  and  $\gamma p \rightarrow p\pi^0\eta$  provide important tools to study the decay dynamics of highly excited baryon resonances. Fig. 2 shows the CB-ELSA  $p\pi^0\pi^0$ -photoproduction cross section up to  $\sqrt{s} \leq 1.8 \text{ GeV}$  [16, 17] together with the result of the fit within the BnGa-partial wave analysis (for further details see [16, 17, 13, 18, 19]). The BnGa-PWA includes in addition to the discussed data set also various data sets on single-meson photoproduction as well as specific waves from elastic  $\pi N$  scattering. In addition, data from Crystal Ball on  $\pi^- p \rightarrow n2\pi^0$  was included in the fit [20]. All three-particle final states are fitted in terms of an event-based maximum likelihood fit, which is the only way to properly take into account all the information included in the correlations between the five variables the reaction depends on. From the fits the properties of the contributing  $N^*$  and  $\Delta^*$  resonances have been extracted and their partial decay widths into the different  $p\pi^0\pi^0$  decay modes, such as  $\Delta(1232)\pi$ ,  $N(\pi\pi)_{S\text{-wave}}$ ,  $P_{11}(1440)\pi$ , and  $D_{13}(1520)\pi$  have been determined (for further details see [16, 17]). Several of these partial widths were not known before. An interesting pattern of partial decays of resonances into  $\Delta\pi$ , not expected by quark model calculations nor by naive phase space arguments, is observed.  $D_{13}$ -decays into  $(\Delta\pi)_{S\text{-wave}}$  are allowed by all selection rules but are observed to be weaker than naively expected. The  $D_{13}(1520)$  decays into  $\Delta\pi$  in D-wave are observed with about the same strength as in S-wave even though D-wave decays should be suppressed at such small momenta ( $\sim 250 \text{ MeV}/c$ ). The  $D_{13}(1700)$   $(\Delta\pi)_{S\text{-wave}}$  decay is observed to be weaker than  $(\Delta\pi)_{D\text{-wave}}$ . For the  $D_{33}(1700)$  two distinct ambiguous solutions have been found; for one of them the S-wave, for the other one the D-wave, dominates. So it remains presently unclear whether only the  $N^*$ -states,  $D_{13}(1520)$  and  $D_{13}(1700)$ , or also the  $\Delta^*$ -states with  $J^P = 3/2^-$  show this unexpected decay pattern. Double polarisation experiments as presently performed

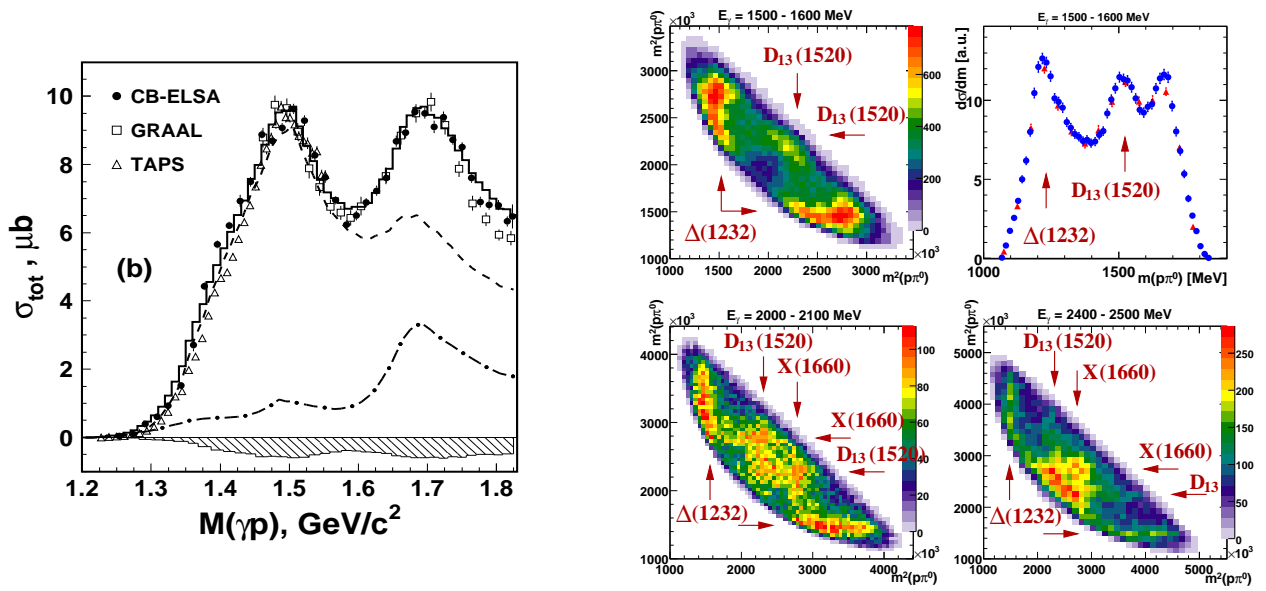


**FIGURE 2.**  $\gamma p \rightarrow p\pi^0\pi^0$ : Left: Total cross section (low energy CB-ELSA data). Solid line: Result of the BnGa-PWA, band below the figure: systematic error. Dashed curve:  $\Delta^+\pi^0 \rightarrow p\pi^0\pi^0$ , dashed-dotted line:  $p(\pi^0\pi^0)_S$  cross section derived from the PWA. The  $D_{33}$  partial wave gives the strongest contribution to the second resonance region, followed by  $D_{13}$ . The  $D_{13} - D_{33}$  interference generates the dip between the second and third resonance region. Right: Dalitz plots and differential cross section distribution in arbitrary units for different tagged photon energy ranges as indicated above the figures (High energy CBELSA/TAPS data).

at the electron stretcher ring ELSA [21] in Bonn are urgently needed.

In addition to the low-energy data also data at higher energies (up to  $\sqrt{s}=2.5$  GeV) have been taken. The existence of baryon cascades, for which the low energy data set provided first evidence is further affirmed by the higher energy data. In the Dalitz plots clear structures due to the  $\Delta(1232)$ ,  $D_{13}(1520)$  and an additional state around 1660 MeV are visible (see Fig. 2). In addition, also the  $f_2(1270)$  and the  $f_0(980)$  contribute. According cascade decays are also observed in the  $p\pi^0\eta$  final state, where e.g. the  $S_{11}(1535)$  and the  $a_0(980)$  contribute in addition to the  $\Delta(1232)$  [22, 24]. The strong occurrence of high mass resonances in the data and in the decay of baryon resonances (PWA) may indicate that QCD prefers to invest in mass rather than in momentum.

## POLARISATION OBSERVABLES

Table 1 shows the 16 observables accessible for photoproduction of single pseudoscalar mesons. For a complete experiment, allowing for a model independent partial wave analysis, 8 carefully chosen observables need to be measured [25].

**TABLE 1.** Observables in single pseudoscalar meson photoproduction. Presently accessible are  $\sigma, \Sigma, E, G$  (blue) using a longitudinally polarized or unpolarized target and a linear, circular or unpolarized photon beam.  $T, P, H, F$  (red): Single and double polarization observables accessible with a polarized or unpolarized beam and transversally polarized target, which is presently in preparation.

Photon		Target			Recoil			Target-Recoil			
		$x$	$y$	$z$	$x'$	$y'$	$z'$	$x'$	$x'$	$z'$	$z'$
unpolarized	$\sigma$	0	$T$	0	0	$P$	0	$T_{x'}$	$-L_{x'}$	$T_{z'}$	$L_{z'}$
linear	$(-\Sigma)$	$H$	$(-P)$	$(-G)$	$O_{x'}$	$(-T)$	$O_{z'}$	$(-L_{z'})$	$(T_{z'})$	$(-L_{x'})$	$(-T_{x'})$
circularly	0	$F$	0	$(-E)$	$(-C_{x'})$	0	$(-C_{z'})$	0	0	0	0

While differential cross sections and the beam asymmetry  $\Sigma$  have been measured for various channels, experiments with a longitudinally polarized target and a circularly or linearly polarized beam have been performed only recently. Experiments with a transversally polarized target are planned for 2010. In contrast to single pseudoscalar meson pho-

toproduction, where 8 carefully chosen observables need to be measured to reach a complete experiment [25], 15 observables [26] have to be determined in case of the photoproduction of two pseudoscalar mesons. This is due to the fact that the reaction is no longer restricted to a single plane; two planes, a reaction and a decay plane, are of importance. As a consequence polarisation asymmetries can also occur if e.g. only the beam is circularly polarised or if only the target is longitudinally polarised. Being restricted to only the reaction plane, those asymmetries do not occur in single pseudoscalar meson photoproduction.

### Measurement of the beam asymmetry $\Sigma$

One of the polarisation observables of interest is the single polarisation observable  $\Sigma$  which will be discussed in the following. In case of a linearly polarised photon beam and an unpolarised target, the cross section for the photoproduction of one respectively two pseudoscalar mesons can be written in the form

$$\frac{d\sigma}{d\Omega} = \left(\frac{d\sigma}{d\Omega}\right)_0 (1 + \delta_l (\Sigma \cos 2\Phi)) , \quad \frac{d\sigma}{d\Omega} = \left(\frac{d\sigma}{d\Omega}\right)_0 (1 + \delta_l (\Sigma \cos 2\Phi + I^S \sin 2\Phi)) \quad (1)$$

where  $\left(\frac{d\sigma}{d\Omega}\right)_0$  denotes the cross section in case of an unpolarised photon beam,  $\delta_l$  the degree of linear polarisation of the photon beam,  $\Sigma$  and  $I^S$  the occurring polarisation observables, where  $I^S$  only occurs in the case with 2 mesons in the final state if the reaction as well as the decay plane are considered.  $\Phi$  is the angle between the polarisation plane and the normal to the reaction plane. In the CBELSA/TAPS experiment the linearly polarised photons are produced

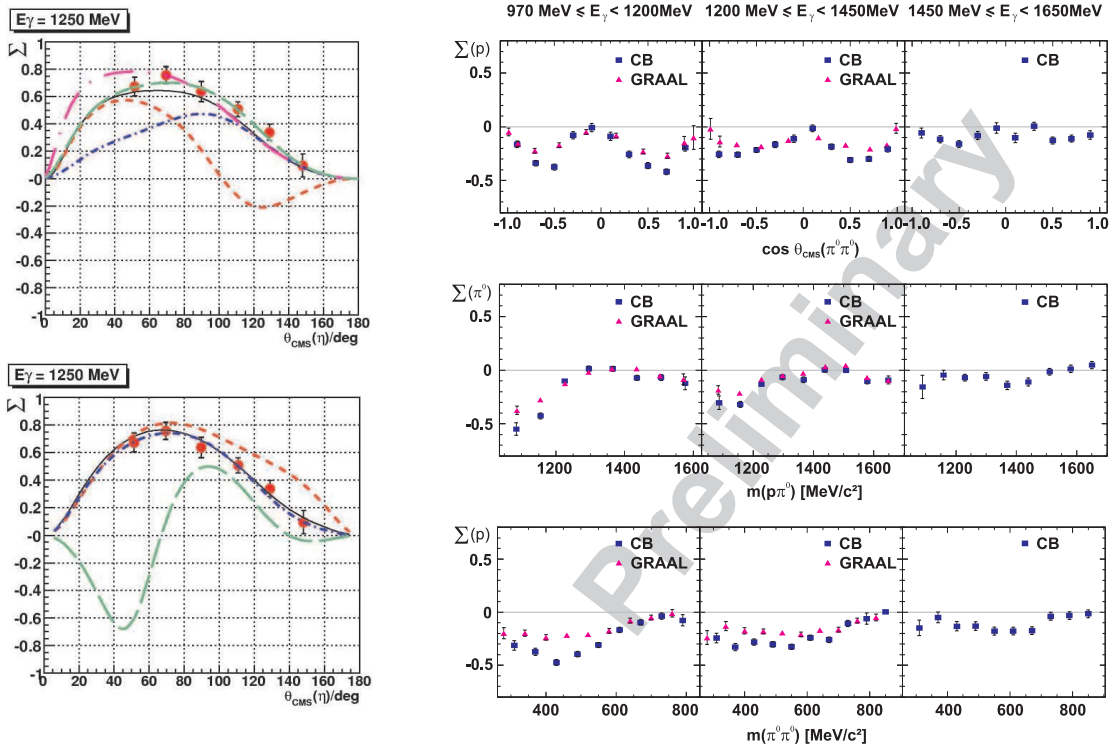


**FIGURE 3.** Left:  $\eta$ -beam asymmetry for  $E_\gamma = (1250 \pm 50)$  MeV [27] together with the description (solid black line) by  $\eta$ -MAID [14] (upper figure) and the BnGa-PWA [13] (lower figure). The broken curves illustrate the effect of “turning off” individual resonances; Long dashed is without  $P_{13}(1720)$ , long dash-dotted without  $P_{11}(1710)$  (no difference to full calculation in BnGa-PWA analysis), short dashed without  $D_{13}(1520)$ , and short dash-dotted without  $D_{15}(1675)$ . Right: Measured beam asymmetries  $\Sigma$  in the reaction  $\bar{\gamma}p \rightarrow p\pi^0\pi^0$ . First row: Beam asymmetries obtained from the  $\Phi$ -distribution of the proton as a function of  $\cos \Theta_{cms}$  of the  $\pi^0\pi^0$  system. Second row: Obtained from the  $\Phi$ -distribution of the  $\pi^0$  as a function of the  $p\pi^0$  invariant mass. Third row: Obtained from the  $\Phi$ -distribution of the proton as a function of the  $\pi^0\pi^0$  invariant mass. The GRAAL data [29] cover incoming photon energies up to 1450 MeV.

via coherent bremsstrahlung of the initial 3.2 GeV electron beam delivered by ELSA off a diamond radiator [27]. Electrons undergoing the bremsstrahlung process are then momentum analysed using a tagging spectrometer consisting of a dipole magnet and a scintillator based detection system. For the given analysis, two data sets were considered, one yielding a maximum degree of polarisation of 49.2% at  $E_\gamma = 1300$  MeV and the other of 38.7% at 1600 MeV. To extract the polarisation observables according to Eq. (1) a fit to the  $\Phi$  distribution of the final state particles was performed. Fig. 3, left shows an example for the beam asymmetry measured for the reaction  $\vec{\gamma}p \rightarrow p\eta$ . The data are compared to the  $\eta$ -MAID and the BnGa-PWA result. In spite of the good agreement between data and both models, the physical content of the two analyses is rather different. In the BnGa-PWA solution [13] the  $P_{13}(1720)$  provides, in the selected mass bin, the strongest contribution. Removing  $P_{13}(1720)$  in the BnGa-PWA fit (without re-adjustment of other parameters) a rather large effect is observed, while the effect is much smaller in  $\eta$ -MAID. In the  $\eta$ -MAID fit on the other hand a significant contribution of the  $P_{11}(1710)$  is found, which did not make a significant contribution in the shown solution of the BnGa-PWA. This indicates that even though the differential cross section and beam asymmetry  $\Sigma$  are both well described, the contributing partial waves may still be rather different. This clearly indicates that further observables need to be measured; observables with polarized beam and polarized target are urgently needed. Fig. 3, right shows preliminary results for the beam asymmetries  $\Sigma$  extracted for the  $\vec{\gamma}p \rightarrow p\pi^0\pi^0$ -channel [28]. Clearly visible are energy and angular dependencies. The beam asymmetry tends to be largest in the lowest energy bin measured. The agreement with the previously published data points from GRAAL [29] is reasonable even though especially in the  $\Sigma(p)(m(\pi^0\pi^0))$ -distributions deviations are observed. These might be due to different areas of the five-dimensional phase space covered by the two experiments. Results for the  $\vec{\gamma}p \rightarrow p\pi^0\eta$ -channel are discussed in [24].

## RECENT DOUBLE POLARISATION MEASUREMENTS

Significant progress in understanding the baryon excitation spectrum can clearly not be expected without further extensive information on polarisation observables. One important step forward is without doubt the measurement of double polarisation observables. First measurements using a longitudinally polarised target and a linearly or circularly polarised photon beam have recently started at ELSA [21] using the setup discussed in the following.

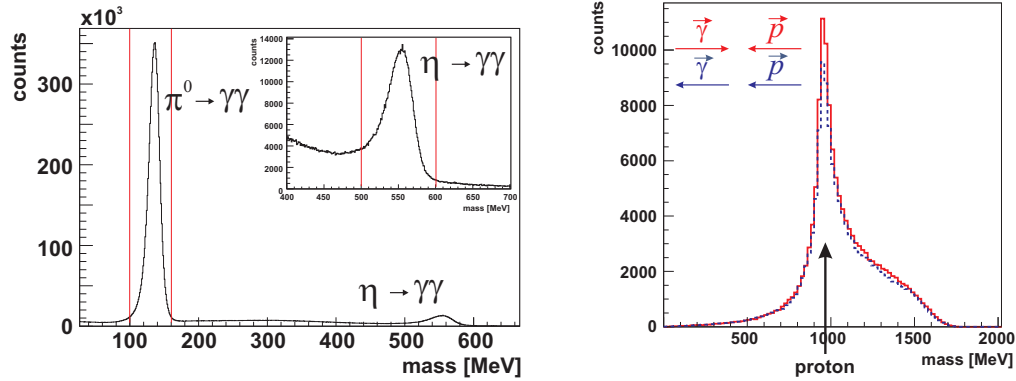
### Experimental setup

The double polarisation measurements have been performed using the Bonn-frozen-spin butanol target [30]. During the measurements a typical mean polarisation of 70% and relaxation times around 600 h have been reached. Circularly polarised photons have been obtained by bremsstrahlung of longitudinally polarised electrons on an amorphous radiator. At 2.4 GeV electron energy an electron beam polarisation  $\sim 65\%$  was obtained at the radiator target. Linearly polarised photons have been obtained using the method of coherent bremsstrahlung off a diamond radiator using an  $e^-$ -beam with an energy of 3.2 GeV. The Crystal Barrel calorimeter consists of 1230 CsI(Tl)-crystals and is complemented by two further calorimeters; the forward detector and the MiniTAPS array. The forward detector consists of 90 CsI(Tl) crystals covering the angular range between  $30^\circ$  and  $12^\circ$ . The MiniTAPS array (216 BaF<sub>2</sub>-crystals) covers the angular range further down to  $1.2^\circ$ . Plastic scintillators are placed in front of the crystals of both forward detectors to identify charged particles. For the forward detector charged identification is provided by a double layer of 180 plastic scintillators of 3 mm thickness, while the front faces of the MiniTAPS BaF<sub>2</sub> crystals are covered by 5 mm plastic scintillator plates. For further charged particle detection a fibre detector consisting of three layers of in total 513 fibres is installed inside the Crystal Barrel calorimeter. The CBELSA/TAPS setup covers  $\sim 96\%$  of the  $4\pi$  solid angle. With the setup discussed data have been taken using the longitudinally polarised frozen spin butanol target and a circularly or linearly polarised photon beam giving access to the double polarisation observables  $E$  and  $G$ .

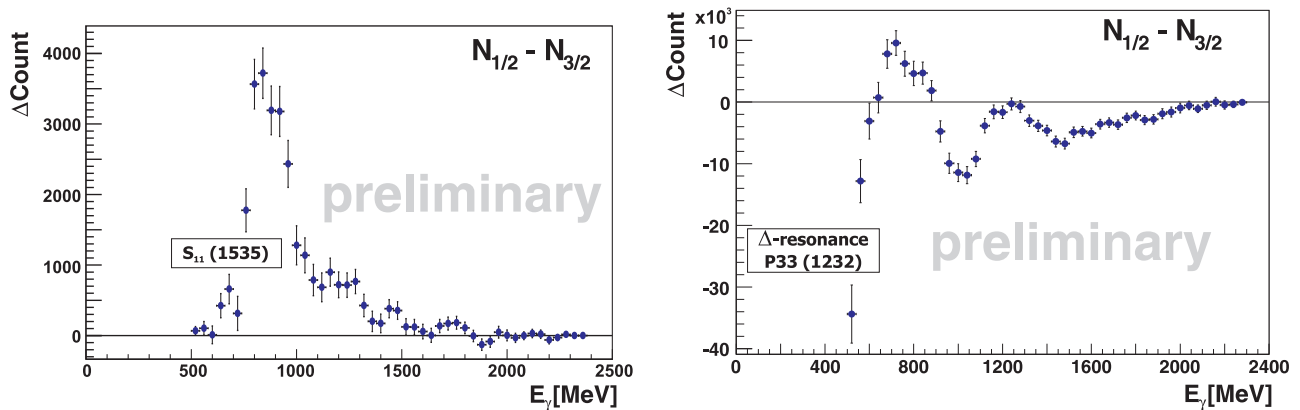
### Measurements with circularly polarized photons

Fig. 4 shows some spectra of the double polarisation data taken with the CBELSA/TAPS experiment. Even though the data selection as well as the calibration is still preliminary Fig. 4 shows clear  $\pi^0$ - and  $\eta$ -signals above a small

background, which will be reduced further by a more refined analysis. Plotting the missing mass distribution for



**FIGURE 4.** Left: Invariant  $\gamma\gamma$ -mass distribution for events with a charged particle and two photons in the final state after a coplanarity and a missing mass cut. Analysis and calibration: preliminary. The vertical (red) lines indicate the  $\pi^0$ - and  $\eta$ -mass cut used. Right: Missing mass distribution for events which are consistent with  $\bar{\gamma}\bar{p} \rightarrow X\eta$ . Events with helicity 1/2 are plotted as solid (red) line, events with helicity 3/2 as dashed (blue) line. A clear count rate difference is observed in the proton mass region. Preliminary analysis and calibration, only part of the statistics shown.



**FIGURE 5.** Raw count rate differences between events with helicity 1/2 and 3/2 ( $\Delta = N_{1/2} - N_{3/2}$ ) for the reaction  $\bar{\gamma}\bar{p} \rightarrow p\eta$  (left) and  $\bar{\gamma}\bar{p} \rightarrow p\pi^0$  (right). This data do neither contain corrections for acceptance nor has the polarization and photon flux been taken into account hence its status is preliminary [31]. Only part of the statistics shown.

events being consistent with  $\bar{\gamma}\bar{p} \rightarrow X\eta$  using the  $\eta$  cut indicated, Fig. 4,right is obtained. The missing mass is shown for events where the spin of photon beam and proton target were aligned parallel in comparison to the ones where are aligned anti-parallel. For events with a missing mass being consistent with the proton, indicating  $\gamma p \rightarrow p\eta$  events, a clear count rate difference is observed; the events with helicity 1/2 dominate over the events with helicity 3/2. Fig.5,left shows this count rate difference as a function of the incoming photon energy. As expected,  $N_{1/2}$  dominates at low energies. This is due to the dominance of the  $S_{11}(1535)$  close to threshold. This behaviour is also clearly visible in all different PWA-predictions for  $\sigma_{1/2} - \sigma_{3/2}$  (see Fig.6,left). Clear differences between the different PWAs occur in the area above  $E_\gamma=1000$  MeV. Particularly interesting is the region around  $E_\gamma=1100$  MeV. While the solution of the BnGa-PWA published in [13] allows within errors for negative values of  $\sigma_{1/2} - \sigma_{3/2}$ , so shown in Fig.5, up to slightly positive values, the MAID solution shows a clear positive value. The main difference between those solutions is a strong contribution of the  $P_{11}(1710)$  in MAID, which is not needed in the BnGa-PWA [13], while in this case the  $P_{13}(1720)$  contributes quite strongly. A very preliminary comparison with the data, which are not yet corrected for acceptance, nor has the polarisation or the flux been taken into account, indicates that this difference might indeed be positive. More information is provided by the according differential distributions, which cover the whole angular range and presently energies up to 2.3 GeV. Fig.5,right shows the according distributions for the  $p\pi^0$  final state. The energy dependent count rate difference  $N_{1/2}-N_{3/2}$  indicates resonance structures, starting at low energies as expected from negative values. Here the  $\Delta(1232)$  dominates. At higher energies the raw count rate difference (preliminary) indicates

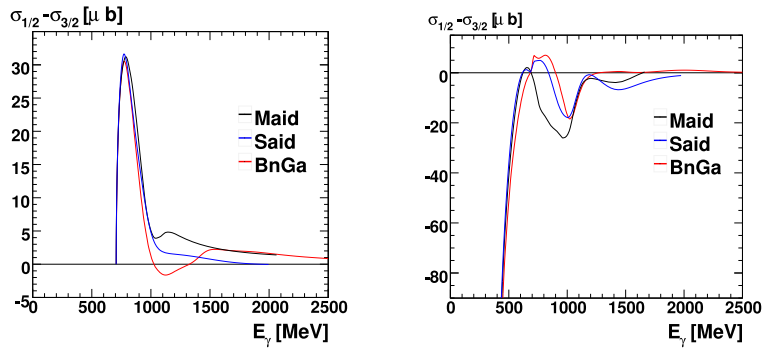


FIGURE 6.  $\sigma_{1/2} - \sigma_{3/2}$ -prediction from BnGa-PWA [13],  $\eta$ -MAID [14] and SAID [15] for  $\bar{\gamma}\bar{p} \rightarrow \bar{p}\eta$  (left),  $\bar{\gamma}\bar{p} \rightarrow \bar{p}\pi^0$  (right).

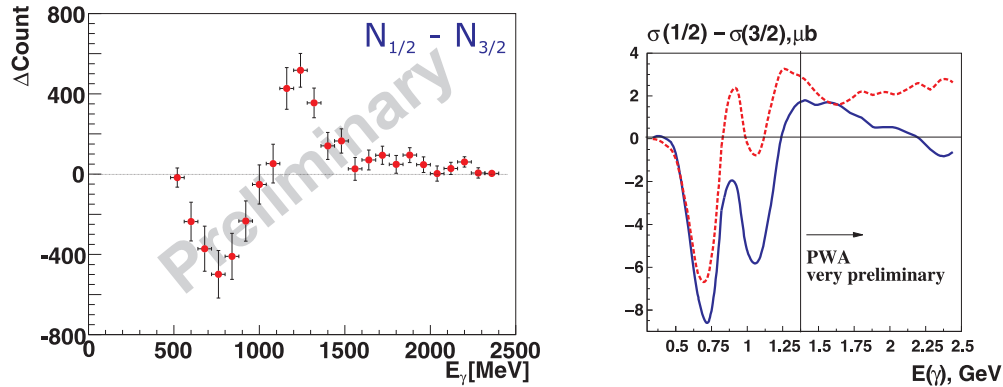


FIGURE 7. Left: Count rate difference of events with helicity 1/2 ( $N_{1/2}$ ) and helicity 3/2 ( $N_{3/2}$ ). The data are not corrected for acceptance, nor has the polarisation or the flux been taken into account, pure raw count rate differences are shown (very preliminary). Right:  $\gamma p \rightarrow p\pi^0\pi^0$ : Predictions for the helicity differences  $\sigma_{1/2} - \sigma_{3/2}$  from the BnGa-PWA for the two ambiguous solutions where the  $D_{33}(1700)$  might either decay dominantly via  $\ell=0$  (dashed, red) or  $\ell=2$  (solid, blue) into  $\Delta\pi$ .

positive as well as negative values. Fig.5,right shows again significant differences between the different PWAs for this final state. The sensitivity of  $\sigma_{1/2} - \sigma_{3/2}$  on the differences between SAID, MAID and BnGa, which include different contributions, already visible in the total cross section is of course even larger in the differential distributions. Again, with the CBELSA/TAPS setup an almost complete angular coverage will be reached for those observables. It should also be mentioned that Fig. 5 shows only part of the available statistics.

Of course also double meson photoproduction is of interest and has been investigated. Fig. 7 shows an example. As discussed before the solution of the BnGa-partial wave analysis shows an ambiguity[16]; the  $D_{33}(1700)$  might either decay dominantly via  $\ell=0$  or  $\ell=2$ . For those two solutions the helicity differences  $\sigma_{1/2} - \sigma_{3/2}$  have been predicted. Large differences in the total as well as in the differential cross sections are observed. First double polarisation data have been taken at ELSA and is presently analysed. A very preliminary result for the raw count rate difference is shown in Fig. 7,left. The spectrum includes only a part of the taken statistics.

## Measurements with linearly polarized photons

Using linearly polarized photons and a longitudinally polarized target the single polarization observable  $\Sigma$  and the double polarization observable  $G$  can be measured simultaneously. Data were taken recently at ELSA, that cover a range in the photon energy from  $E_\gamma=0.4$  to 1.35 GeV. In a first preliminary analysis events due to the reactions  $\gamma p \rightarrow p\eta$  and  $\gamma p \rightarrow p\pi^0$  are reconstructed from events with 3 clusters in the calorimeters only, leading to a restricted angular coverage. This will be significantly improved by a more refined analysis. Experiments using linear polarized photons and a longitudinally polarised target lead to a distribution of events which is no longer  $\phi$ -symmetric but shows

a modulation in the azimuthal angle  $\phi$ .

$$N(\theta, \phi) = (N_C + N_H) \cdot (1 - \Sigma \cdot p_{lin}^\gamma \cos(2\phi)) + \frac{N_H}{N_C + N_H} \cdot p_z^{target} p_{lin}^\gamma \cdot G \cdot \sin(2\phi)$$

The polarization observable  $G$  can be extracted by fitting the observed  $\phi$ -dependence if also the target polarization, the degree of linear polarization of the beam and the dilution factor  $\frac{N_H}{N_C + N_H}$  is known. A preliminary dilution factor has been determined from an additional analysis of data which have been taken using a hydrogen and a carbon target. Fig. 8 shows an example of the obtained preliminary results (for further details and results see [32]). The results are shown in comparison to the partial wave predictions from the BnGa-PWA, MAID and SAID analysis showing again significant differences. Clearly, also this new data will provide important new information for the PWA-analyses.

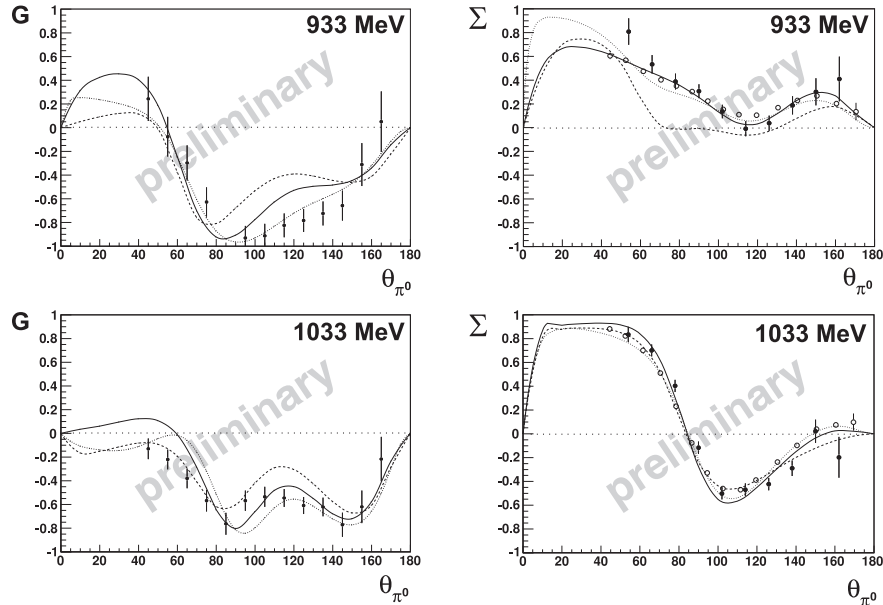


**FIGURE 8.** Preliminary results for the polarisation observable  $\Sigma$  and the double polarisation observable  $G$  for the reaction  $\gamma p \rightarrow p\pi^0$ , preliminary dilution factor taken into account. The two energy bins shown have a width of 33 MeV. Solid line: SAID, dashed line: MAID, dotted line: BnGa-PWA

We acknowledge financial support from the Deutsche Forschungsgemeinschaft (DFG) within SFB/TR16.

## REFERENCES

1. S. Capstick and N. Isgur, Phys. Rev. D **34** 2809 (1986).
2. L. Y. Glozman *et al.*, Phys. Rev. D **58** 094030 (1998).
3. U. Löring *et al.*, Eur. Phys. J. A **10** 395, 447 (2001).
4. S. Capstick, W. Roberts, Prog. Part. Nucl. Phys. **45** S241 (2000).
5. E. Oset *et al.*, Int. J. Mod. Phys. A **20** 1619 (2005).
6. M. Döring, E. Oset, D. Strottman, Phys. Rev. C **73**, 045209 (2006).
7. M. F. M. Lutz, E. E. Kolomeitsev, Nucl. Phys. A **755** 29 (2005).
8. V. Crede *et al.*, Phys. Rev. C **80**, 055202 (2009)
9. E. Klempt and J. M. Richard, arXiv:0901.2055 [hep-ph].
10. V. Crede *et al.*, Phys. Rev. Lett. **94**, 012004 (2005)
11. J. Ajaka *et al.*, Phys. Rev. Lett. **81**, 1797 (1998).
12. B. Krusche *et al.*, Phys. Rev. Lett. **74**, 3736 (1995).
13. A. V. Anisovich *et al.*, Eur. Phys. J. A **25**, 427 (2005)
14. W. T. Chiang *et al.*, Phys. Rev. C **68**, 045202 (2003)
15. R. A. Arndt *et al.*, Phys. Rev. C **66**, 055213 (2002)
16. U. Thoma *et al.*, Phys. Lett. B **659** 87 (2008)
17. A. V. Sarantsev *et al.*, Phys. Lett. B **659** 94 (2008).
18. A. V. Anisovich, A. V. Sarantsev, Eur. Phys. J. A **30**, 427 (2006).
19. This conference, contribution of A. V. Anisovich.
20. S. Prakhov *et al.*, Phys. Rev. C **69** (2004) 045202.
21. W. Hillert, Eur. Phys. J. A **28S1**, 139 (2006).
22. I. Horn *et al.*, Phys. Rev. Lett. **101** 202002 (2008),
23. I. Horn *et al.*, Eur. Phys. J. A **38** 173 (2008).
24. E. Gutz *et al.*, Eur. Phys. J. A **35**, 291 (2008),  
this conference, contribution of E. Gutz,
25. W. T. Chiang, F. Tabakin, Phys. Rev. C **55**  
2054 (1997).
26. W. Roberts, T. Oed, Phys. Rev. C **71** 055201 (2005).
27. D. Elsner *et al.*, Eur. Phys. J. A **33**, 147 (2007),  
Eur. Phys. J. A **39** 373 (2009).
28. V. Sokhoyan, PhD thesis, Bonn (in preparation).
29. Y. Assafiri *et al.*, Phys. Rev. Lett. **90** 222001 (2003).
30. Bradtke *et al.*, NIM A 436 (1999) 430
31. M. Gottschall, PhD thesis, Bonn (in preparation).
32. This conference, contribution of A. Thiel.